Protonation Sites of Isolated Fluorobenzene Revealed by IR Spectroscopy in the Fingerprint Range

Otto Dopfer,*,† Nicola Solcà,† Joel Lemaire,‡ Philippe Maitre,‡ Maria-Elisa Crestoni,§ and Simonetta Fornarini§

Institut für Physikalische Chemie, Universität Würzburg, Am Hubland, D-97074 Würzburg, Germany, Laboratoire de Chimie Physique, UMR8000-Université Paris-Sud 11, Faculte des Sciences d' Orsay, Bâtiment 350, 91405 Orsay Cedex, France, and Dipartimento di Studi di Chimica e Tecnologia delle Sostanze Biologicamente Attive, Università di Roma La Sapienza, Piazzale A. Moro 5, 00185 Roma, Italy

Received: June 1, 2005; In Final Form: July 15, 2005

Protonated fluorobenzene ions ($C_6H_6F^+$) are produced by chemical ionization of C_6H_5F in the cell of a FT-ICR mass spectrometer using either CH_5^+ or $C_2H_5^+$. The resulting protonation sites are probed by IR multiphoton dissociation (IRMPD) spectroscopy in the 600−1700 cm^{-1} fingerprint range employing the free electron laser at CLIO (Centre Laser Infrarouge Orsay). Comparison with quantum chemical calculations reveals that the IRMPD spectra are consistent with protonation in para and/or ortho position, which are the thermodynamically favored protonation sites. The lack of observation of protonation at the F substituent, when CH_5^+ is used as protonating agent, is attributed to the low-pressure conditions in the ICR cell where the ions are produced. Comparison of the $C_6H_6F^+$ spectrum with IR spectra of C_6H_5F and $C_6H_7^+$ reveals the effects of both protonation and H → F substitution on the structural properties of these fundamental aromatic molecules.

1. Introduction

The protonation of aromatic molecules is a central process in biology and organic chemistry. In particular, protonated aromatic molecules (henceforth denoted AH^+) are frequently invoked as reactive intermediates in fundamental organic ionic reaction mechanisms.[1,2] For example, they appear as σ complexes (Wheland intermediates) in electrophilic aromatic substitution (EAS) reactions, namely the most important reaction class of aromatic molecules. It is well recognized that fundamental properties of ion−molecule reactions, such as energetics and dynamics, sensitively depend on the solvation environment, because of the strong interaction between the charge of the reacting ionic species and the surrounding solvent molecules. The detailed understanding of the impact of solvation on the properties of such ion−molecule reaction mechanisms requires the characterization of AH^+ ions under isolated and controlled microsolvation conditions. In contrast to the large body of spectroscopic information acquired in the condensed phase,[3,4] until recently, all experimental information about isolated AH^+ ions was almost exclusively based on mass spectrometric experiments,[5−7] which provide only indirect and often ambiguous structural information. The radiolytic approach to the characterization of arenium ions in the gas phase at atmospheric pressure is more informative but still relies on reactivity probes.[5,6] Spectroscopic information to determine, for example, directly the preferred protonation sites in isolated AH^+ ions have been lacking because of the difficulties encountered in the production of sufficient concentrations. Recent progress in the development of sensitive IR photodissociation schemes[8−10] allowed for the first time to spectroscopically characterize isolated[11,12] and microsolvated[13] AH^+ ions. The systems investigated so far include AH^+ ions with A=benzene,[12,14−16] (para-halogenated) phenols,[13,17−20] fluorobenzene,[11,21] phenylsilane,[22] and benzoic acid.[23] These studies mainly addressed the question of the preferred protonation site(s), the photofragmentation behavior, and the influence of stepwise microsolvation in a polar and nonpolar environment.

Two major IR photodissociation strategies have successfully been applied to AH^+ ions. The first technique employs modern, low-intensity, optical parametric oscillator (OPO) laser systems in the frequency range 2500−4000 cm^{-1} to drive one-photon IR photodissociation (IRPD) of AH^+-L_m cluster ions. This approach is based on the evaporation of one or more of the weakly bound ligands upon resonant absorption of a single photon (messenger technique).[13,15] This method can also be applied to break weak chemical bonds in certain AH^+ isomers but usually fails to dissociate common AH^+ ions because the energy of a single IR photon is insufficient to break strong covalent bonds.[11] This shortcut is overcome by the second technique, which utilizes high-intensity free electron lasers (FEL) in the frequency range 50−2500 cm^{-1} to drive IR multiphoton photodissociation (IRMPD) processes of AH^+ ions.[12] This IRMPD approach has recently been applied to AH^+ ions with A = benzene,[12] phenylsilane,[22] and protonated benzoic acid,[23] and is used in the present work to characterize protonated fluorobenzene.

The potential energy surface (PES) of protonated fluorobenzene ($C_6H_6F^+$) has been studied in detail by quantum chemical techniques.[11,24−32] The minimum structures and the PES calculated at the B3LYP/6-311G(2df,2pd) level are shown in Figures 1 and 2, respectively.[11] Protonation can occur at the aromatic ring (**1**−**4**) or at the F atom (**5**), leading to the formation of carbenium and fluoronium ions, respectively. Their

* Corresponding author. E-mail: dopfer@phys-chemie.uni-wuerzburg.de. Fax: (+49) 931-888-6378. Phone: (+49) 931-888-6377.
† Universität Würzburg.
‡ Université Paris-Sud 11.
§ Università di Roma *La Sapienza.*

10.1021/jp052907v CCC: $30.25
Published on Web 08/17/2005

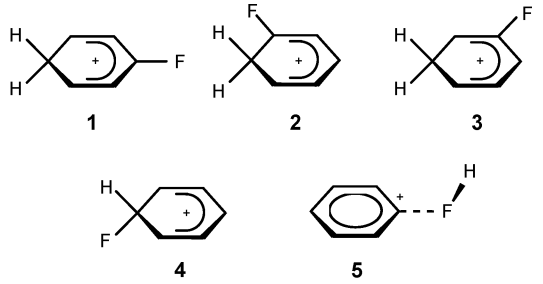

Figure 1. Isomeric structures of protonated fluorobenzene ($C_6H_6F^+$). Protonation can occur at the para (**1**), ortho (**2**), meta (**3**), and ipso (**4**) positions as well as at the F atom (**5**).

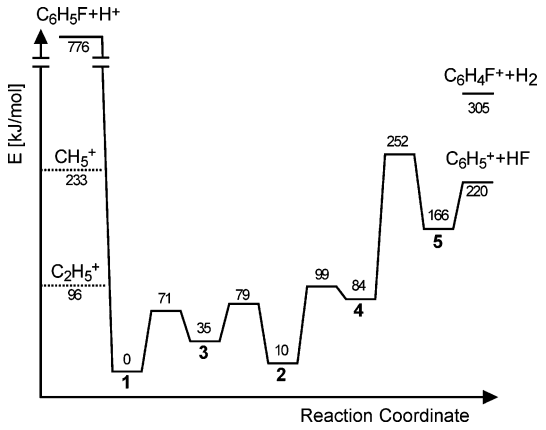

Figure 2. Schematic energy profile displaying the relevant stationary points of the potential energy surface of protonated fluorobenzene ($C_6H_6F^+$) calculated at the B3LYP/6-311G(2df,2pd) level.[11] Experimental excess energies for protonation with CH_5^+ and $C_2H_5^+$ are indicated by dotted lines.[11,42]

relative energies increase in the order **1** < **2** ≪ **3** ≪ **4** ≪ **5**, reflecting the ortho/para directing nature of the F substituent in EAS reactions. **5** is separated from **1**−**4** by a high barrier, whereas the barriers between **1**−**4** are small. All minima on the PES are σ complexes and no stable π complex could be located. As protonation at the F substituent considerably destabilizes the strong C−F single bond of C_6H_5F, **5** is best described as a weakly bound ion−dipole complex between the phenyl cation and HF, $C_6H_5^+$−FH, with a relatively low dissociation energy of the order of 50 kJ/mol. Consequently, dehydrofluorination is by far the lowest dissociation channel for **1**−**5**, whereas H_2 loss is significantly higher in energy (Figure 2).

Early experimental information about the structure of protonated fluorobenzene isomers was provided by ^1H and ^{19}F NMR spectroscopy in superacid solutions.[33,34] A static σ complex **1** was found at low temperature, whereas complete scrambling of all ring protons was observed in the high-temperature limit due to rapid intramolecular 1,2 H-shift. Only the carbenium isomers **1**−**3** were detected in these solutions, and no experimental evidence was presented for the existence of a π complex or the fluoronium isomer **5**.

Until recently, all experimental information about $C_6H_6F^+$ isolated in the gas phase came from the radiolytic approach[35,36] and mass spectrometric techniques,[24,26,27,31,32,37−41] including high-pressure mass spectrometry, proton-transfer equilibria measurements, metastable decay analysis, kinetic energy release measurements, and collision-induced dissociation (CID) experiments. The protonation sites of $C_6H_6F^+$ generated by either chemical ionization (CI) or electron ionization (EI) were found to strongly depend on the experimental ion source conditions, such as temperature, pressure, and the protonating agent and precursor used for the CI and EI processes, respectively. Both thermodynamic and kinetic factors strongly influence the observed isomer ratios. The proton affinities (PA) of C_6H_5F for generating **1** and **5** were determined as 755.9 and 577 ± 24 kJ/mol, respectively,[24,42] in good agreement with the calculations. Although **5** is substantially less stable than **1**−**4**, significant concentrations of **5** could be generated by near resonant proton transfer, that is, using a Brønsted acid for protonation with similar or slightly smaller PA, such as CH_5^+ (PA_{CH_4} = 544 kJ/mol).[42] Once stable **5** is formed, its conversion into the more stable isomers **1**−**4** is strongly hindered by a high isomerization barrier (Figure 2). In contrast, **5** cannot be produced in significant abundance using protonating agents with significantly lower or higher PA, such as H_3^+ or $C_2H_5^+$ (PA_{H_2} = 422 kJ/mol, $PA_{C_2H_4}$ = 681 kJ/mol).[42] In the first case, the large excess energy involved in the proton-transfer step creates internally hot **5**, which results in quantitative unimolecular dissociation via HF loss. In the latter case, the proton-transfer reaction generating **5** is endothermic, preventing direct protonation at the F atom (e.g., Figure 2 for $C_2H_5^+$).

Recently, the protonation sites of C_6H_5F have spectroscopically been characterized under isolated and microsolvated conditions by single-photon IRPD of either bare $C_6H_6F^+$ or weakly bound $C_6H_6F^+$−$(N_2)_2$ clusters and monitoring the following fragmentation reactions:[11,21]

$$C_6H_6F^+ + h\nu \rightarrow C_6H_5^+ + HF \quad (1)$$

$$C_6H_6F^+-(N_2)_2 + h\nu \rightarrow C_6H_6F^+ + 2N_2 \quad (2)$$

Cold $C_6H_6F^+$ ions were prepared in a supersonic plasma expansion created by electron impact in the high-pressure region of a molecular beam. As the $C_6H_6F^+$ ions were generated by CI using CH_4, significant concentrations of both **5** and the carbenium isomers **1** and/or **2** were present in the generated $C_6H_6F^+$ beam. In the first experiment,[11] IRPD spectra of $C_6H_6F^+$ were obtained in the C−H and F−H stretch ranges (2540−4050 cm^{-1}) by coupling an OPO laser with a tandem quadrupole mass spectrometer. The low intensity of the available OPO laser (I < 200 kW/cm^2; E < 1 mJ/pulse) enabled only one-photon absorption processes to be observed. Consequently, isomer **5** of $C_6H_6F^+$ could selectively be detected in the IRPD spectrum, because only for this isomer the available photon energy (3000 cm^{-1} ∼ 36 kJ/mol) was sufficient to drive the dehydrofluorination reaction (Figure 2). Spectroscopic signatures of the more stable carbenium isomers, although certainly present in high concentrations in the prepared $C_6H_6F^+$ ion beam, were not detected.[11] The analysis of the C−H and F−H stretch spectrum of **5** yielded detailed information about its structure, distribution of the excess charge, and bonding mechanism.[11] In particular, it provided unambiguous spectroscopic confirmation of the $C_6H_5^+$−FH structure of **5** predicted theoretically.

In an effort to selectively detect the more stable carbenium isomers **1** and **2**, IRPD spectra of weakly bound $C_6H_6F^+$−$(N_2)_2$ clusters were recorded in a separate experiment.[21] For this purpose, microsolvated $C_6H_6F^+$ cluster ions were generated by CI using H_2 to significantly suppress the production of **5**. The attachment of N_2 ligands had the following two major implications (messenger approach).[15,43,44] First, the required energy to drive the IRPD process is substantially reduced because the lowest dissociation channel corresponds to the rupture of the weak intermolecular bonds of $C_6H_6F^+$ to the inert N_2 ligands (D_0 ∼ 10 kJ/mol) rather than breaking intramolecular bonds.

As a consequence, the carbenium isomers of $C_6H_6F^+$ could selectively be detected by single photon IRPD via the process described in eq 2. Second, the $C_6H_6F^+-(N_2)_2$ clusters are rather cold, because their internal energy has to be below the lowest dissociation energy ($E_{int} < D_0$) to survive the passage from the ion source to the octopole trap where IRPD is performed. The analysis of the IRPD spectra of $C_6H_6F^+-(N_2)_2$ in the C−H stretch range revealed absorptions characteristic for the aliphatic CH_2 group (sp^3 hybridization of C, $\sigma_{CH} \sim 2840$ cm^{-1}) and the aromatic CH groups (sp^2 hybridization of C, $\sigma_{CH} \sim 3120$ cm^{-1}). Detailed comparison with quantum chemical calculations demonstrated that mainly **1** and **2** contributed to the $C_6H_6F^+-(N_2)_2$ spectrum, consistent with the ortho/para directing nature of the F substituent in EAS reactions.

The present work reports IRMPD spectra of $C_6H_6F^+$ generated in an ion cyclotron resonance (ICR) instrument using the free electron laser at CLIO (Centre Laser Infrarouge Orsay). It extends the previous spectroscopic interrogations of $C_6H_6F^+$ in various aspects.[11,20,21] First, the spectral range covered in the present study (600−1700 cm^{-1}, so-called fingerprint region) is complementary to the previous work using an OPO laser (2540−4050 cm^{-1}), yielding valuable new information on vibrational frequencies. In particular, comparison with the corresponding spectra of neutral fluorobenzene[45] and protonated benzene[12,46] will reveal the effects of both protonation and H → F substitution on the structural properties of the arenium ion. Second, the much higher intensity of the FEL (∼1 W) compared to that of the OPO laser (<20 mW) opens the possibility to drive multiphoton absorption processes, which are exploited in the present work to observe IRMPD. Hence, in contrast to the previous OPO studies, all $C_6H_6F^+$ isomers produced can be detected by monitoring the following two relevant IRMPD processes:

$$C_6H_6F^+ + nh\nu \rightarrow C_6H_5^+ + HF \quad (3a)$$

$$\rightarrow C_6H_4F^+ + H_2 \quad (3b)$$

Third, whereas most previous studies employed high-pressure ion sources for $C_6H_6F^+$ generation, the ions are created in the present approach in a low-pressure ICR cell (typically 5×10^{-9} to 5×10^{-8} mbar) via CI using mass-selected CH_5^+ or $C_2H_5^+$ ions. This is an important aspect, as the ion source conditions are crucial for the produced $C_6H_6F^+$ isomer ratio. In addition to the protonation site and its spectroscopic consequences, the present study will also address the differences in the fragmentation branching ratios observed for collisional and infrared activation (CID versus IRMPD).

2. Experimental and Computational Methods

The experimental setup couples a mobile FT-ICR mass spectrometer analyzer (MICRA) with tuneable IR laser radiation from the FEL at CLIO. Details of the coupling of MICRA[47] with the FEL[48] were described previously.[10,49] The $C_6H_6F^+$ ions are generated in the ICR cell by chemical ionization of C_6H_5F using mass-selected CH_5^+ or $C_2H_5^+$ ions. To this end, a 200 ms CH_4 pulse at $p = 9 \times 10^{-7}$ mbar is introduced into the cell and ionized by a 200 ms electron pulse. After mass selection of either CH_5^+ or $C_2H_5^+$, a C_6H_5F pulse with 200 ms length and $p = 2 \times 10^{-7}$ mbar is injected into the cell. The $C_6H_6F^+$ ions generated by exothermic proton transfer are mass selected and subsequently irradiated for 1 s with the FEL radiation (∼1 W), which is composed of 8 μs macropulses (25 Hz), each divided into 500 micropulses (few picoseconds long, 16 ns apart). Finally, a mass spectrum is recorded at each wavelength of the IR laser to collect the parent ions as well as the daughter ions, which arise from either IRMPD or unimolecular dissociation. At the present experimental conditions, fragmentation of $C_6H_6F^+$ occurs mainly into the lowest energy fragment channel, corresponding to HF loss, but loss of H_2 is also observed as a minor fragment channel (eq 3).

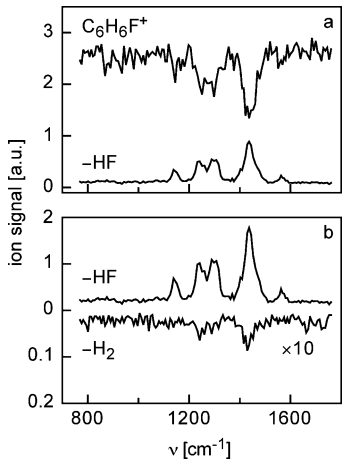

Figure 3. (a) $C_6H_6F^+$ parent ion and $C_6H_5^+$ fragment ion signal (HF loss) in arbitrary units as a function of the IR laser frequency. (b) Comparison of the $C_6H_5^+$ (HF loss) and the $C_6H_4F^+$ (H_2 loss) fragment ion signals as a function of the IR laser frequency. The H_2 loss channel is about a factor 25 less intense than the HF loss channel. All spectra are obtained using CH_5^+ as protonating agent.

Density functional theory calculations are carried out at the B3LYP/6-311G(2dp,2df) level to characterize the PES of protonated fluorobenzene,[50] with the main focus on the stability and IR spectral properties of isomers **1**−**5**.[11] Previous calculations revealed that this theoretical level reliably describes the PES of $C_6H_6F^+$, with a quality similar to that of the MP2/6-311G(2dp,2df) level.[11] All coordinates are allowed to relax for the search of stationary points on the PES. Energies are corrected for the effects of zero-point energy. Harmonic frequencies are scaled by a factor of 0.96 to account for anharmonicity. For comparison, similar calculations are carried out for C_6H_5F and $C_6H_7^+$.

3. Results and Discussion

Figure 3a compares the $C_6H_6F^+$ parent ion signal with that of the strongest fragment ion signal ($C_6H_5^+$, HF loss) as a function of the IR laser frequency. Clearly, there is a 1:1 correspondence between the $C_6H_6F^+$ depletion and $C_6H_5^+$ appearance signals with respect to both the positions and the widths of the resonances. For the strongest resonance near 1450 cm^{-1}, the depletion is as large as 40%, indicating the high efficiency of the IRMPD process. Figure 3b demonstrates that the ratio for the $C_6H_5^+$ and $C_6H_4F^+$ fragment ion channels is of the order of 25:1, clearly showing the dominance of HF loss over the energetically less favorable H_2 loss under the present experimental conditions. In addition, the ratio appears to be roughly independent of the IR frequency. Similar observations were previously reported for IRMPD of $Fe^+(CH_3OCH_3)_2$, where dissociation into the two major fragment channels (loss of CH_3 and CH_4) occurred in a constant ratio, independent of the vibrational resonance excited in the parent ion.[10] In current models to describe the IRMPD process, sequential heating of the parent ion occurs via the successive absorption of single IR photons intermediated by intramolecular vibrational relaxation. This relatively slow heating process favors dissociation into the lowest energy fragment channel with branching ratios indepen-

dent of the laser frequency.[51] According to the dissociation energies given in Figure 2, HF (H_2) loss for cold **1** requires the absorption of $n = 13$ ($n = 18$) photons with $\nu = 1450$ cm^{-1}, respectively. Similarly to IRMPD, both CID experiments of ring-protonated $C_6H_6F^+$ (**1**, **2**) at low collision energies and unimolecular dissociation favor HF loss over H_2 elimination.[26,32,39] On the other hand, CID at high collision energies induces preferentially H_2 loss rather than HF loss.[27,31,40] Apparently, high excitation of **1** and **2** via a single excitation event leads to direct ejection of H_2, which is fast on the time scale required for isomerization via the high barrier toward HF elimination (Figure 2). On the other hand, heating of **1** and **2** in the IRMPD process via the sequential absorption of multiple IR photons appears to be slow enough to facilitate isomerization and subsequent fragmentation into the lowest energy fragmentation channel. Figure 3a also shows that there is a significant frequency-independent background signal in the $C_6H_5^+$ channel (4% of parent ions). This background is large only when CH_5^+ is used for $C_6H_6F^+$ generation. It can be ascribed to unimolecular decay of hot $C_6H_4F^+$ ions, which is fast ($\tau \sim 10^{-5}$ s)[32] on the time scale of the present experiment ($\sim$1 s). Unimolecular dissociation may arise from both the fluoronium isomer **5** (vide infra) and the carbenium isomers **1** and **2**.

Figure 4 compares the experimental IRMPD spectrum of $C_6H_6F^+$ in the investigated spectral range (600−1700 cm^{-1}) with linear IR absorption spectra calculated for isomers **1**−**5**. As the observed IRMPD spectrum is relatively independent of the Brønsted acid employed for formation of $C_6H_6F^+$ (CH_5^+ or $C_2H_5^+$), only the one recorded using CH_5^+ is shown. The positions and widths of the transitions observed (A−F) are collected in Table 1. The suggested vibrational and isomer assignments are based on the comparison with the calculated spectra. For comparison, Table 1 also lists the calculated frequencies and IR intensities as well as the symmetry species of the involved normal modes.

First, the isomer assignments are considered. Inspection of Figure 4 immediately reveals rather convincing agreement between the IRMPD spectrum and the spectra predicted for isomers **1** and **2** with respect to both the band positions and the relative band intensities. On the basis of the calculations, it is difficult to decide whether both isomers or only one of them contributes to the experimental spectrum (vide infra). Both isomers are by far the most stable minima on the $C_6H_6F^+$ PES and are therefore expected to be generated in significant abundances. In contrast, the IR spectra of isomers **3**−**5** differ qualititatively from the measured IRMPD spectrum, as is evidenced by the lack of the intense theoretical transitions (marked by filled circles in Figure 4) in the experimental spectrum. Hence, the abundances of isomers **3**−**5** are concluded to be small and below the detection limit.

The absence (or low concentration) of **3** and **4** in the ion source may be rationalized by (i) their smaller stabilization energies compared to those of **1** and **2** and (ii) their low isomerization barriers toward **1** and/or **2** (Figure 2). The absence of **5** in the IRMPD spectra when $C_2H_5^+$ is used for $C_6H_6F^+$ production is expected, because the PA of C_6H_5F at the F atom is smaller than that of C_2H_4 (Figure 2), preventing efficient generation of **5** in the ion source. On the other hand, the lack of detection of **5** in IRMPD spectra when CH_5^+ is used for $C_6H_6F^+$ production may, at first glance, be somewhat surprising because this isomer was previously produced in significant abundance in high-pressure CI ion sources using this Brønsted acid. However, our efforts in creating substantial amounts of cold species **5** in the low-pressure ICR cell have not been successful when CH_5^+ is used as protonating agent. This observation may be rationalized by the low pressure in the ICR cell, which prevents efficient cooling of **5** via three-body collisions. Apparently, most of **5** produced in the early stage of the ion−molecule reaction sequence decays via unimolecular

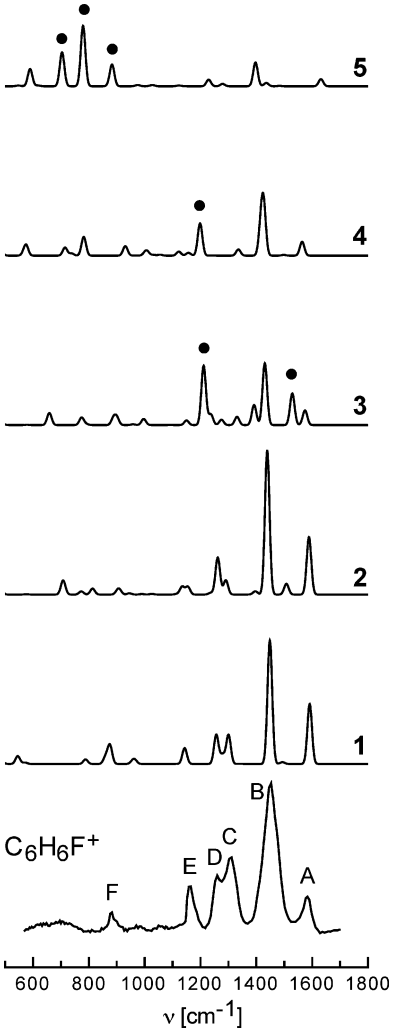

Figure 4. Comparison of the experimental IRMPD spectrum of $C_6H_6F^+$ (using CH_5^+ as protonating agent) monitored in the HF loss channel with linear IR absorption spectra of isomers **1**−**5** calculated at the B3LYP/6-311G(2df,2pd) level using a convolution width of 20 cm^{-1} and a scaling factor of 0.96. The lack of detection of the intense bands predicted for isomers **3**−**5** (indicated by filled circles) in the measured spectrum strongly suggests that mainly isomers **1** and/or **2** contribute to the experimental spectrum. The positions, widths, and assignments of the transitions observed in the IRMPD spectrum (A−F) are listed in Table 1.

TABLE 1: Maxima, Widths (fwhm), and Assignments of the Transitions Observed in the IRMPD Spectra of $C_6H_6F^+$ (Figure 4) along with the Theoretical Predictions (in cm^{-1})

band	position	width	*p*-$C_6H_6F^+$ (**1**)[a]	*o*-$C_6H_6F^+$ (**2**)[a]
A	1583	36	1591 (177/a_1) σ_{CC}	1589 (169/a′) σ_{CC}
B	1451	56	1450 (183/b_2) σ_{CC}	1439 (425/a′) σ_{CC}
			1447 (190/a_1) σ_{CC}	
C	1308	54	1300 (86/a_1) σ_{CF}	1290 (42/a′) σ_{CF}
D	1260	32	1257 (86/a_1) β_{CH2}	1262 (109/a′) β_{CH2}
E	1161	30	1143 (47/a_1) β_{CH}	1154 (23/a′) β_{CH}
				1134 (23/a′) β_{CH}
F	881	31	876 (55/b_1) ring	909 (13/a′) ring
			860 (20/a_1) ring	902 (7/a″) ring

[a] IR intensities (km/mol) and symmetry species of the vibrations are listed in parentheses.

TABLE 2: Comparison of Experimental and Calculated Frequencies (in cm^{-1}) of Selected Normal Modes of C_6H_5F, $C_6H_6F^+$ (Isomer 1), and $C_6H_7^+$ [a]

mode[b]		C_6H_5F		*p*-$C_6H_6F^+$ (**1**)		$C_6H_7^+$	
		exp[c]	calc	exp	calc	exp[d]	calc
9a (a_1)	β_{CH}	1156	1130 (10)	1161	1143 (47)	1190	1166 (24)
15 (b_2)	β_{CH}/β_{CF}	405	391 (2)		410 (8)	1190	1160 (18)
7a (a_1)	σ_{CF}	1239	1213 (88)	1308	1300 (86)		
scissor	β_{CH_2}			1260	1257 (86)	1225	1228 (112)
19a (a_1)	σ_{CC}	1499	1470 (77)	1451	1447 (190)		1425 (27)
19b (b_2)	σ_{CC}	1460	1431 (2)	1451	1450 (183)	1438	1426 (180)
8a (a_1)	σ_{CC}	1603	1575 (46)	1583	1591 (177)	1585	1640 (76)
8b (b_2)	σ_{CC}	1597	1578 (9)		1494 (6)		1512 (2)

[a] IR intensities (in km/mol) are listes in parentheses. [b] Symmetry species in the C_{2v} point group are listed in parentheses. [c] References 53 and 54. [d] References 46 and 12.

dissociation before interacting with the IR irradiation, giving rise to the constant background in the HF loss channel (Figure 3a). Mass spectra obtained at short delay times after ion generation feature a large unimolecular decay peak for HF loss, supporting the conclusion of fast decay of hot **5**.[32] The fact that the unimolecular dissociation background is low when $C_2H_5^+$ is used for $C_6H_6F^+$ generation confirms this interpretation, because under these conditions **5** is not produced in measurable abundance in the ion source. In addition to HF loss, proton transfer of **5** with background C_6H_5F may also deplete the population of **5**. The possibility that the intense low-frequency features predicted for **5** between 600 and 800 cm^{-1} are not observed in the experimental spectrum due to the nature of the IRMPD process is unlikely, because the low dissociation energy of **5** requires the absorption of only $n = 7$ photons with $\nu = 700$ cm^{-1}. This should give rise to a relatively high IRMPD efficiency, even though IVR rates might be expected to be small in the early stage of the multiple photon absorption process for vibrations with low frequency. Indeed, the lack of detection of **5** in the present ICR experiments should not be unexpected. A quite similar behavior has been found in the dissociative proton transfer of α,α,α-trifluorotoluene that is triggered under ICR conditions by protonation at a fluorine atom, namely, the most basic site in this molecule.[52]

After assigning the transitions A−F observed in the IRMPD spectrum of $C_6H_6F^+$ to isomers **1** and/or **2**, we consider their vibrational interpretation. In general, the good agreement between the observed and calculated spectra with respect to both band positions and relative IR intensities enables straightforward vibrational assignments (Table 1, Figure 4). On the other hand, the intense features in the IR spectra calculated for **1** and **2** are rather similar in frequency and IR intensity (Figure 4, Table 1) within the resolution of the experimental approach (∼30 cm^{-1}), preventing an unambiguous separation of the contributions of both isomers to the IRMPD spectrum. The high-frequency transitions A and B occurring at 1583 and 1451 cm^{-1} are attributed to C−C stretch vibrations, σ_{CC}. Band C at 1308 cm^{-1} corresponds to the C−F stretch mode, σ_{CF}, whereas band D at 1260 cm^{-1} arises from the scissoring motion of the methylene group, β_{CH_2}. Band E at 1161 cm^{-1} can be assigned to in-plane C−H bending motions, β_{CH}, whereas band F at 881 cm^{-1} mainly arises from an out-of-plane ring deformation. The width of the most narrow transitions in the IRMPD spectrum is of the order of 30 cm^{-1} (Table 2), which is typical for isolated transitions observed in IRMPD spectra of related molecules in this size range.[12] Contributions to the width arise from both unresolved rotational structure and cross anharmonicities associated with sequence transitions involved in the IRMPD process. Several bands may additionally be broadened due to overlapping transitions arising from isomers **1** and **2**. The deviations of the calculated from the experimental frequencies (12 ± 9 cm^{-1}) are less than 28 cm^{-1} and significantly smaller than the experimental widths of the transitions.

In an effort to unravel the effects of both protonation and H → F substitution, Figure 5 compares the structural parameters and the charge distributions of C_6H_5F, isomer **1** of $C_6H_6F^+$, and $C_6H_7^+$. Major effects of (para-)protonation on C_6H_5F include a contraction of the C−F bond ($\Delta R = -0.049$ Å), a deformation of the aromatic ring toward a 1,4-cyclohexadienyl-type structure, and an elongation of the C−H bond at the protonation site ($\Delta R = 0.023$ Å). The excess charge of the attached proton in **1** is largely delocalized over the whole molecule. The six protons carry around 70% of the positive charge ($q_H \sim 0.12$ e), whereas the C atoms and the CF group are less charged (∼0.05 e). Comparison between $C_6H_7^+$ and **1** demonstrates that H → F substitution slightly enhances the deformation of the aromatic ring induced by protonation. In general, the arenium ions are best described as (substituted) pentadienyl cations bridged by a methylene group.[25]

The structural implications upon protonation and H → F substitution are directly transferring into the corresponding IR spectra. Experimental IR spectra of C_6H_5F,[45,53,54] $C_6H_6F^+$, and $C_6H_7^+$,[46] recorded in the fingerprint region are compared in Figure 6 and Table 2 along with simulated linear IR absorption spectra (isomer **1** is selected for $C_6H_6F^+$). The IRMPD spectrum of $C_6H_7^+$ is similar in appearance to the one recorded previously with the same experimental approach[12] but displays a somewhat better spectral resolution and more spectral features. The nomenclature for the vibrational modes employed in Table 2 and Figure 6 follows the Wilson notation for vibrations of benzene and its derivatives.[53,55] In line with the predicted trend, the frequency of the in-plane bend, ν_{9a}, increases in the order C_6H_5F → **1** → $C_6H_7^+$. The substituent-sensitive in-plane bend, ν_{15}, overlaps with ν_{9a} for $C_6H_7^+$ at around 1190 cm^{-1}. However, H → F substitution transforms this mode into the in-plane C−F bend and shifts its frequency down to around 400 cm^{-1} for both C_6H_5F and **1**. The contraction of the C−F bond upon para-protonation of C_6H_5F results in a significant increase in the C−F stretch frequency, ν_{7a}, from 1239 to 1308 cm^{-1}. As predicted by the calculations, the frequency of the scissoring mode of the aliphatic methylene group in the arenium ions increases substantially upon H → F substitution from 1225 to 1260 cm^{-1}. According to the calculations, para-protonation of C_6H_5F nearly removes the splitting between the two C−C stretch modes ν_{19a} and ν_{19b}, leads to an IR enhancement of the weaker ν_{19b} component, and keeps the average frequency of the ν_{19} doublet roughly constant. This trend appears to be confirmed by the experimental IR spectra when taking into account that the blue part of the broad $\nu_{19a/b}$ band (band B) in the experimental $C_6H_6F^+$ spectrum arises from isomer **1**. The red part of band B at 1451 cm^{-1} is ascribed to the corresponding contribution of isomer **2** with slightly lower frequency (Table 1). As an alternative scenario, the broad band B may be explained as the ν_{19a} and ν_{19b} modes of only isomer **1**, with an experimental splitting larger than predicted. In this case, isomer **2** would not contribute to the observed IRMPD spectrum. As the stabilization energies of **1** and **2** are quite similar ($\Delta E = 10$ kJ/mol, Figure 2) and both isomers are separated by large isomerization barriers ($V \sim 70$ kJ/mol), the interpretation that both **1** and **2** are detected in the measured IRMPD spectrum in Figure 4 is presently favored. Both the calculations and the experimental spectra reveal that H → F substitution slightly increases the frequency of $\nu_{19a/b}$. The highest frequency C−C stretch modes in these

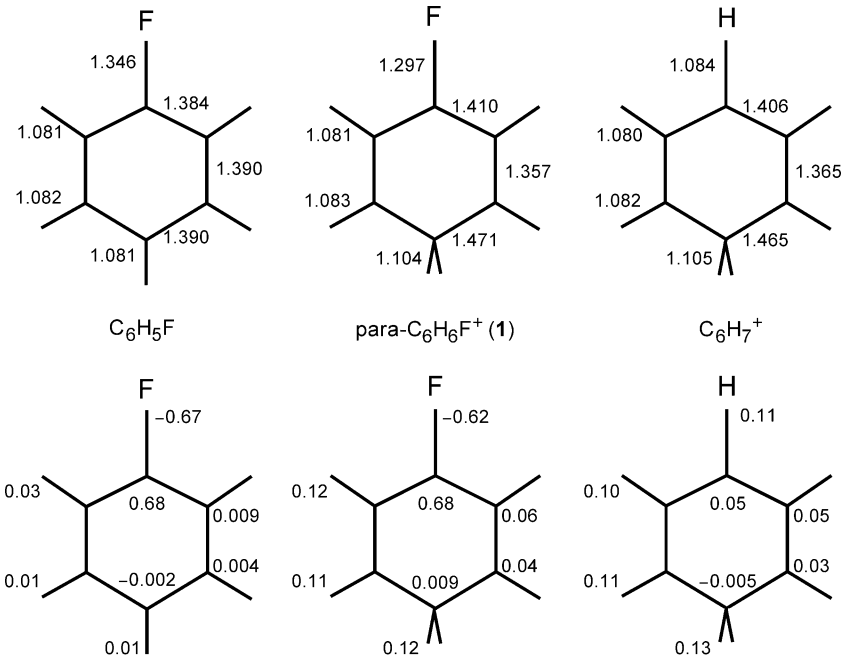

Figure 5. Structural parameters (in Å) and charge distributions (atoms-in-molecules population analysis) of C_6H_5F, $C_6H_6F^+$ (para-protonated isomer **1**), and $C_6H_7^+$ evaluated at the B3LYP/6-311G(2df,2pd level).

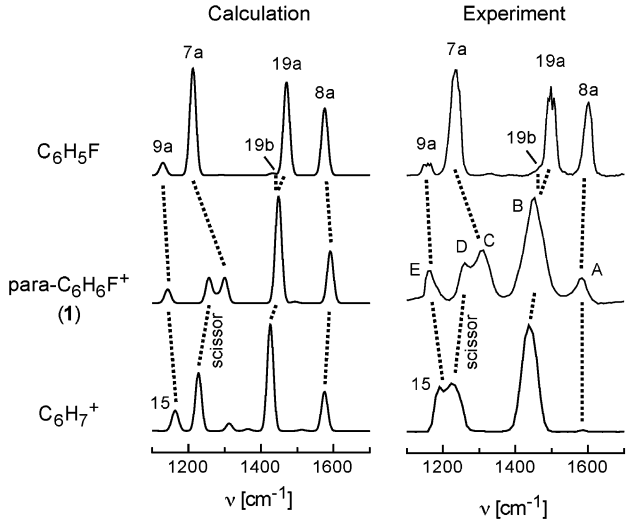

Figure 6. Comparison of linear IR absorption spectra of C_6H_5F, $C_6H_6F^+$ (para-protonated isomer **1**), and $C_6H_7^+$ calculated at the B3LYP/6-311G(2df,2pd) level with the corresponding experimental IR absorption spectrum of C_6H_5F[45] and IRMPD spectra of $C_6H_6F^+$ (Figure 4) and $C_6H_7^+$.[46]

simple benzene derivatives correspond to the $\nu_{8a/b}$ doublet, of which only the ν_{8a} component has significant IR intensity. Interestingly, this is the only vibration in the investigated spectral range, for which the predicted protonation effect is opposite to the observed trend: the protonation shifts calculated for both **1** and **2**, $\Delta\nu_{8a} = +16$ and $+14$ cm^{-1}, substantially deviate from the measured shift, $\Delta\nu_{8a} = -20$ cm^{-1}. In addition, also the relative IR intensity of this band is significantly lower in the IRMPD spectrum. Both effects are attributed to the details of the IRMPD process, which results in an underestimated frequency and IR intensity compared to the predicted linear IR absorption spectrum data. The fact that ν_{8a} can hardly be seen in the IRMPD spectrum of $C_6H_7^+$ despite its relatively large IR intensity confirms the conclusion that the efficiency for the IRMPD process is relatively low for this particular mode.[12] Finally, it is noted that the spectroscopic implications of protonation and H → F substitution in the F−H and C−H stretch ranges were described in detail previously.[11,20,21]

4. Concluding Remarks

The IR spectrum of protonated fluorobenzene ions ($C_6H_6F^+$), produced by chemical ionization using either CH_5^+ or $C_2H_5^+$ in a FT-ICR mass spectrometer, has been recorded for the first time in the 600−1700 cm^{-1} fingerprint range, utilizing IRMPD spectroscopy employing the free electron laser at CLIO. Comparison with density functional calculations reveals that the IRMPD spectrum is consistent with protonation in the para and/or ortho position (**1** and/or **2**), which are the thermodynamically favored protonation sites. Despite considerable effort to protonate fluorobenzene at the F substituent by near-resonant proton transfer using CH_5^+, F-protonated $C_6H_6F^+$ isomers (**5**) could not be detected. The lack of **5** in the IRMPD spectrum is attributed to the low-pressure conditions in the ICR cell, which prevent efficient collisional stabilization prior to fast unimolecular decay of this isomer. In general, good agreement is observed between the linear IR absorption spectra simulated for **1** and **2** (employing a scaling factor of 0.96) and the measured IRMPD spectrum of $C_6H_6F^+$, with average deviations of around 12 cm^{-1} between calculated and experimental vibrational frequencies. Comparison with the IR spectra of C_6H_5F and $C_6H_7^+$ has unravelled the effects of both protonation and H → F substitution on the structural properties of these aromatic molecules. The combined experimental and theoretical strategy will be employed soon to probe the chemical properties of a variety of protonated aromatic molecules to elucidate subtle substitution effects of isolated reactive intermediates with relevance to fundamental organic reaction mechanisms.

Acknowledgment. This work was supported by the CNRS, the University of Paris-Sud and especially its laser facility POLA, the Italian MIUR, and the *Deutsche Forschungsgemeinschaft* (DO 729/2-2). We thank Jean-Michel Ortega and coworkers at the CLIO facility for their support during the experiments. Financial support by the European Commission (project IC 009-04) is gratefully acknowledged (travel grants

to M.E.C. and O.D.). O.D. is supported by a Heisenberg Fellowship (DO 729/1-2) and the *Fonds der Chemischen Industrie*.

References and Notes

(1) Smith, M. B.; March, J. *Advanced Organic Chemistry: Reactions, Mechanisms, and Structure*, 5th ed.; Wiley: New York, 2001.

(2) Carey, F. A.; Sundberg, R. J. *Advanced Organic Chemistry*; Plenum Press: New York, 1995.

(3) Brouwer, D. M.; Mackor, E. L.; MacLean, C. Arenonium Ions. In *Carbonium Ions*; Olah, G. A., Schleyer, P. v. R., Eds.; Wiley: New York, 1970; Vol. II.

(4) Koptyug, V. A. *Top. Curr. Chem.* **1984**, *122*, 1.

(5) Fornarini, S. *Mass Spectrom. Rev.* **1996**, *15*, 365.

(6) Fornarini, S.; Crestoni, M. E. *Acc. Chem. Res.* **1998**, *31*, 827.

(7) Kuck, D. *Mass Spectrom. Rev.* **1990**, *9*, 583.

(8) Okumura, M.; Yeh, L. I.; Lee, Y. T. *J. Chem. Phys.* **1985**, *83*, 3705.

(9) Bieske, E. J.; Dopfer, O. *Chem. Rev.* **2000**, *100*, 3963.

(10) Maitre, P.; Le Caer, S.; Simon, A.; Jones, W.; Lemaire, J.; Mestdagh, H.; Heninger, M.; Mauclaire, G.; Boissel, P.; Prazeres, R.; Glotin, F.; Ortega, J. M. *Nucl. Instrum. Methods, Sect. A* **2003**, *507*, 541.

(11) Solcà, N.; Dopfer, O. *J. Am. Chem. Soc.* **2003**, *125*, 1421.

(12) Jones, W.; Boissel, P.; Chiavarino, B.; Crestoni, M. E.; Fornarini, S.; Lemaire, J.; Maitre, P. *Angew. Chem., Int. Ed.* **2003**, *42*, 2057.

(13) Solcà, N.; Dopfer, O. *Chem. Phys. Lett.* **2001**, *342*, 191.

(14) Chiavarino, B.; Crestoni, M. E.; Fornarini, S. *J. Phys. Org. Chem.* **2004**, *17*, 957.

(15) Solcà, N.; Dopfer, O. *Angew. Chem., Int. Ed.* **2002**, *41*, 3628.

(16) Solcà, N.; Dopfer, O. *Chem. Eur. J.* **2003**, *9*, 3154.

(17) Solcà, N.; Dopfer, O. *J. Am. Chem. Soc.* **2004**, *126*, 1716.

(18) Solcà, N.; Dopfer, O. *J. Chem. Phys.* **2004**, *120*, 10470.

(19) Solcà, N.; Dopfer, O. *J. Chem. Phys.* **2004**, *121*, 769.

(20) Solcà, N.; Dopfer, O. *Chem. Phys. Chem.* **2005**, *6*, 434.

(21) Solcà, N.; Dopfer, O. *Angew. Chem., Int. Ed.* **2003**, *42*, 1537.

(22) Chiavarino, B.; Crestoni, M. E.; Fornarini, S.; Lemaire, J.; MacAleese, L.; Maitre, P. *Chem. Phys. Chem.* **2005**, *6*, 437.

(23) Oomens, J.; von Helden, G.; Meijer, G. *J. Phys. Chem. A* **2004**, *108*, 8273.

(24) Mason, R.; Milton, D.; Harris, F. *J. Chem. Soc., Chem. Commun.* **1987**, 1453.

(25) Bader, R. F. W.; Chang, C. *J. Phys. Chem.* **1989**, *93*, 5095.

(26) Hrusak, J.; Schröder, D.; Weiske, T.; Schwarz, H. *J. Am. Chem. Soc.* **1993**, *115*, 2015.

(27) Mason, R. S.; Parry, A. J.; Milton, D. M. P. *J. Chem. Soc., Faraday Trans.* **1994**, *90*, 1373.

(28) Maksic, T. B.; Kovacevic, B.; Kovacek, D. *J. Phys. Chem. A* **1997**, *101*, 7446.

(29) Szulejko, J. E.; Hrusak, J.; McMahon, T. B. *J. Mass. Spectrom.* **1997**, *32*, 494.

(30) Wiberg, K. B.; Rablen, P. R. *J. Org. Chem.* **1998**, *63*, 3722.

(31) Mason, R. S.; Anderson, P. D. J.; Williams, C. M. *J. Chem. Soc., Faraday Trans.* **1998**, 2549.

(32) Schröder, D.; Oref, I.; Hrusak, J.; Weiske, T.; Nikitin, E. E.; Zummack, W.; Schwarz, H. *J. Phys. Chem. A* **1999**, *103*, 4609.

(33) Olah, G. A.; Mo, Y. K. *J. Org. Chem.* **1973**, *38*, 3212.

(34) Olah, G. A.; Kiovsky, T. E. *J. Am. Chem. Soc.* **1967**, *89*, 5692.

(35) Speranza, M.; Cacace, F. *J. Am. Chem. Soc.* **1977**, *99*, 3051.

(36) Cacace, F.; Speranza, M. *J. Am. Chem. Soc.* **1976**, *98*, 7299.

(37) Lau, Y. K.; Kebarle, P. *J. Am. Chem. Soc.* **1976**, *98*, 7452.

(38) Speranza, M.; Sefcik, M. D.; Henis, J. M. S.; Gaspar, P. P. *J. Am. Chem. Soc.* **1977**, *99*, 5583.

(39) Tkaczyk, M.; Harrison, A. G. *Int. J. Mass Spectrom. Ion Processes* **1990**, *100*, 133.

(40) Tkaczyk, M.; Harrison, A. G. *Int. J. Mass Spectrom. Ion Processes* **1994**, *132*, 73.

(41) Lorquet, J. C.; Lorquet, A. J. *J. Phys. Chem. A* **2001**, *105*, 3719.

(42) Hunter, E. P. L.; Lias, S. G. *J. Phys. Chem. Ref. Data* **1998**, *27*, 413.

(43) Yeh, L. I.; Okumura, M.; Myers, J. D.; Price, J. M.; Lee, Y. T. *J. Chem. Phys.* **1989**, *91*, 7319.

(44) Dopfer, O. *Z. Phys. Chem.* **2005**, *219*, 125.

(45) NIST.; Linstrom, P. J.; Mallard, W. G. *NIST Chemistry WebBook*; NIST Standards and Technology, Gaithersburg MD, 20899 (http://webbook.nist.gov), 2001.

(46) Dopfer, O.; et al. Unpublished data.

(47) Mauclaire, G.; Lemaire, J.; Boissel, P.; Bellec, G.; Heninger, M. *Eur. J. Mass Spectrom.* **2004**, *1*, 155.

(48) Prazeres, R.; Glotin, F.; Insa, C.; Jaroszynski, D. A.; Ortega, J. M. *Eur. Phys. J. D* **1998**, *3*, 87.

(49) Lemaire, J.; Boissel, P.; Heninger, M.; Mauclaire, G.; Bellec, G.; Mestdagh, H.; Simon, A.; Le Caer, S.; Ortega, J. M.; Glotin, F.; Maitre, P. *Phys. Rev. Lett.* **2002**, *89*, 273002.

(50) Frisch, M. J.; Trucks, G. W.; Schlegel, H. B.; Scuseria, G. E.; Robb, M. A.; Cheeseman, J. R.; Zakrzewski, V. G.; Montgomery, J. A.; Stratman, R. E.; Burant, J. C.; Dapprich, S.; Millam, J. M.; Daniels, A. D.; Kudin, K. N.; Strain, M. C.; Farkas, O.; Tomasi, J.; Barone, V.; Cossi, M.; Cammi, R.; Menucci, B.; Pomelli, C.; Adamo, C.; Clifford, S.; Ochterski, J.; Petersson, G. A.; Ayala, P. Y.; Cui, Q.; Morokuma, K.; Malick, D. K.; Rabuck, D.; Raghavachari, K.; Foresman, J. B.; Cioslowski, J.; Ortiz, J. V.; Stefanov, B. B.; Liu, G.; Liashenko, A.; Piskorz, P.; Komaromi, I.; Gomperts, R.; Martin, R. L.; Fox, D. J.; Keith, T.; Al-Laham, M. A.; Peng, C. Y.; Nanayakkara, A.; Gonzales, C.; Challacombe, M.; Gill, P. M. W.; Johnson, B. G.; Chen, W.; Wong, M. W.; Andres, J. L.; Gonzales, C.; Head-Gordon, M.; Replogle, E. S.; Pople, J. A. *Gaussian 98*, revision A.7; Gaussian, Inc.: Pittsburgh, PA, 1998.

(51) Ervin, K. M. *Chem. Rev.* **2001**, *101*, 391.

(52) Aschi, M.; Chiavarino, B.; Crestoni, M. E.; Fornarini, S. *J. Phys. Chem.* **1996**, *100*, 19859.

(53) Varsanyi, G. *Assignments for Vibrational Spectra of Seven Hundred Benzene Derivatives*; Wiley: New York, 1974; Vol. 1.

(54) Lipp, E. D.; Seliskar, C. J. *J. Mol. Spectrosc.* **1981**, *87*, 255.

(55) Wilson, E. B. *Phys. Rev.* **1934**, *45*, 706.